Cord blood-derived neuronal cells by ectopic expression of Sox2 and c-Myc

Alessandra Giorgetti[a,1,2], Maria C. N. Marchetto[b,1], Mo Li[c,1], Diana Yu[b], Raffaella Fazzina[a], Yangling Mu[b], Antonio Adamo[a], Ida Paramonov[a], Julio Castaño Cardoso[a], Montserrat Barragan Monasterio[a], Cedric Bardy[b], Riccardo Cassiani-Ingoni[a], Guang-Hui Liu[c], Fred H. Gage[b,3], and Juan Carlos Izpisua Belmonte[a,c,3]

[a]Center of Regenerative Medicine in Barcelona, 08003 Barcelona, Spain; [b]Laboratory of Genetics, Salk Institute for Biological Studies, La Jolla, CA 92037; and [c]Gene Expression Laboratory, Salk Institute for Biological Studies, La Jolla, CA 92037

Contributed by Fred H. Gage, June 7, 2012 (sent for review March 10, 2012)

The finding that certain somatic cells can be directly converted into cells of other lineages by the delivery of specific sets of transcription factors paves the way to novel therapeutic applications. Here we show that human cord blood (CB) CD133$^+$ cells lose their hematopoietic signature and are converted into CB-induced neuronal-like cells (CB-iNCs) by the ectopic expression of the transcription factor Sox2, a process that is further augmented by the combination of Sox2 and c-Myc. Gene-expression analysis, immunophenotyping, and electrophysiological analysis show that CB-iNCs acquire a distinct neuronal phenotype characterized by the expression of multiple neuronal markers. CB-iNCs show the ability to fire action potentials after in vitro maturation as well as after in vivo transplantation into the mouse hippocampus. This system highlights the potential of CB cells and offers an alternative means to the study of cellular plasticity, possibly in the context of drug screening research and of future cell-replacement therapies.

neurons | reprogramming | stem cells

The fate of adult somatic cells is not fixed rigidly and can be reprogrammed by experimental manipulation. The generation of induced pluripotent stem cells (iPSCs) represents the most dramatic evidence that the epigenome of somatic cells are remarkably plastic (1). Recently, it has been reported that fibroblasts can be converted by ectopic expression of defined transcription factors into postmitotic neurons (2–9), neural progenitors (10, 11), and self-renewing neural stem cells (NSCs) (12, 13). However, most reported methods rely on the use of multiple transcription factors and the use of fibroblasts as donor cells.

Here we investigate if cord blood (CB) stem cells can be induced to acquire a neuronal phenotype by using only one transcription factor. It has been previously shown that stem cell populations are more amenable to reprogramming than other somatic cells, probably as a result of their preexisting epigenetic state (14, 15). Moreover, because of their biological characteristics and availability, CB cells as a donor cell type could offer clear logistic advantages vs. other adult somatic cell types (16, 17). These cells can be collected without any risk for the donor and are young cells carrying minimal somatic mutations.

Strikingly, we show that forced expression of Sox2 is sufficient to convert CB CD133$^+$ cells into induced neuronal progenitor (NP)-like cells, a conversion process that is augmented by the coexpression of c-Myc. Sox2 is highly expressed in adult NSCs, is one of the earliest functional markers of neuroectodermal specification in the embryo, and plays a key role in the neural lineage specification (18–20). We show that Sox2-transduced CB cells acquire a distinct neuronal morphology and express multiple neuronal markers in vitro, and that they can be expanded for as many as 25 passages when cultured in permissive condition culture. Moreover, we show that CB-induced neuronal-like cells (CB-iNCs) are able to differentiate in vitro and in vivo into mature neurons that generate action potentials. Our findings provide a proof of principle that human blood cells can be converted into iNCs and offer a complementary paradigm for investigating the molecular mechanisms that underlie direct lineage conversion between somatic cell types.

Results

Sox2 Is Sufficient for Conversion of CB CD133$^+$ Cells into CB-iNCs. CB CD133$^+$ cells were isolated by using CD133 immunoselection (purity range of 92–97%; Fig. S1*A*) and infected with Sox2 retroviral vector (infection efficiency, 20–30%; Fig. S1*B*). To exclude the presence of contaminating rare NP or neural crest (NC) cells within the starting population, we performed an extensive characterization of CD133$^+$ fraction by quantitative real-time (qRT)-PCR and immunocytochemistry. In agreement with previous data, CB CD133$^+$ cells were negative or showed a very low level of early neural markers such as Mash1, Nkx2.2, Sox1, Pax6, Nestin, Otx1, Otx2, NeuroD1, and Doublecortin (Dcx) (21) (Fig. S2 *A* and *B*). Although low levels of mRNA of Sox10 and Snail were observed in a few samples, we could not detect any cells positive for SOX10 or the low-affinity neurotrophin receptor p75NRT by immunofluorescence or FACS analysis (Fig. S2 *C*–*E*). CB CD133$^+$ cells were also negative for other NC markers such as Slug, Ngn1, and Pax3 (Fig. S2 *C* and *D*). Moreover, CD133$^+$ cells did not spontaneously give rise to neuronal cells when maintained under neural culture conditions for a long period (21, 22).

Our initial attempts to convert Sox2-infected CB cells into neurons by using standard neural condition cultures were unsuccessful and infected CD133$^+$ cells underwent apoptosis. Instead, we found that coculture with irradiated human foreskin fibroblasts (i.e., HFF-1 cells) in the presence of bFGF (23) (Fig. 1*A*) were permissive for the survival of Sox2-transduced CB cells. By 3 wk after infection, these conditions led to the appearance of one or two colonies from 3×10^4 CD133$^+$ cells infected (conversion efficiency of 0.004–0.008%). Despite numerous attempts in parallel, we were unable to derive colonies by using the CD133-negative fraction of CB.

Immunocytochemistry analysis showed that the colonies at the earliest passage (i.e., passage 0) were negative for the pluripotency markers OCT4, NANOG, SSEA3, TRA-1–60, and TRA-1–81, as well as alkaline phosphatase (ALP; Fig. 1*B* and Fig. S3*A*). Instead, cells positive for neural progenitor markers TUJ-1, PAX6, and DCX were observed, although the resulting cells showed an immature neuronal morphology (Fig. S3*A*). To gain insight into whether the conversion process occurs by first passing through an intermediate pluripotent state (10, 24), infected CB CD133$^+$ cells

Author contributions: A.G., M.C.N.M., M.L., F.H.G., and J.C.I.B. designed research; A.G., M.C.N.M., M.L., D.Y., R.F., Y.M., A.A., I.P., J.C.C., M.B.M., C.B., R.C.-I., and G.-H.L. performed research; F.H.G. contributed new reagents/analytic tools; A.G., M.C.N.M., M.L., D.Y., Y.M., A.A., I.P., J.C.C., C.B., R.C.-I., and G.-H.L. analyzed data; and A.G., M.C.N.M., M.L., D.Y., Y.M., C.B., F.H.G., and J.C.I.B. wrote the paper.

The authors declare no conflict of interest.

Data deposition: The data reported in this paper have been deposited in the Gene Expression Omnibus (GEO) database, www.ncbi.nlm.nih.gov/geo (accession no. GSE38431).

[1]A.G., M.C.N.M., and M.L. contributed equally to this work.

[2]Present address: Inbiomed, 20009 Gipuzkoa, Spain.

[3]To whom correspondence may be addressed. E-mail: belmonte@salk.edu or gage@salk.edu.

This article contains supporting information online at www.pnas.org/lookup/suppl/doi:10.1073/pnas.1209523109/-/DCSupplemental.

Downloaded at Palestinian Territory, occupied on December 18, 2021

www.manaraa.com

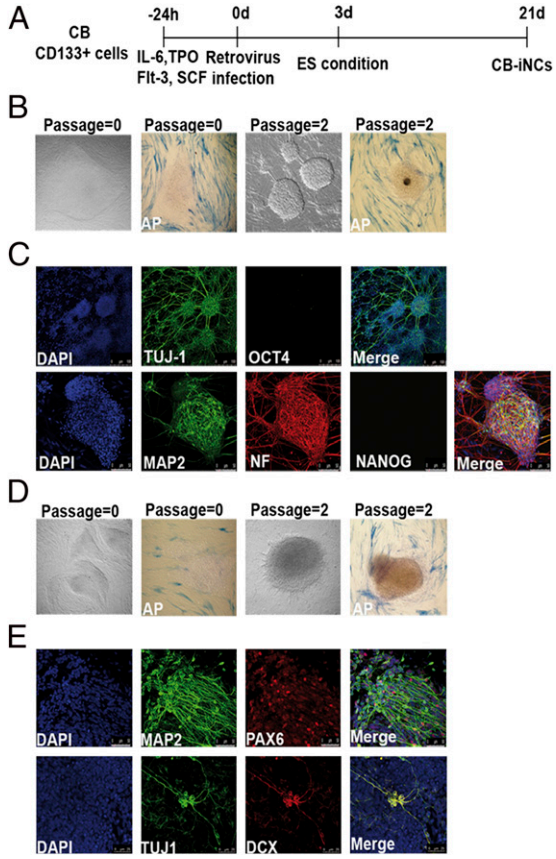

Fig. 1. Images related to CB-iNCs derivation and characterization. (*A*) Timeline of CB CD133$^+$ stem cell conversion into neuronal-like cells. (*B*) Representative phase-contrast images of passage-0 and passage-2 CB-iNCs generated by overexpression of only Sox2 and relative alkaline phosphatase (AP) staining. (*C*) Sox2 CB-iNCs expressed TUJ-1, microtubule-associated protein 2 (MAP2), and NF but were negative for OCT4 and NANOG. Blue indicates nuclei stained with DAPI. (Scale bars: *Upper*, 50 μm; *Lower*, 100 μm.). (*D*) Representative phase contrast images of passage-0 and passage-2 CB-iNCs generated with Sox2 and c-Myc and relative AP staining. (*E*) The colonies contained neuronal cells positive for TUJ-1, MAP2, PAX6, and DCX. Blue indicates nuclei stained with DAPI. (Scale bar, 50 μm.)

were evaluated for the expression of TRA-1–60 and TRA-1–81 at different time points during the conversion process [days (d) 7, d13, and d17]. As shown in Fig. S3*B*, no cells positive for these pluripotency markers were detectable.

Interestingly, after a few passages, the colonies acquired a more complex cytoarchitecture (Fig. 1*B*). Colonies at passage 2 were already composed of cells with a typical neuronal morphology and expressed TUJ-1, Neurofilament (NF), and microtubule-associated protein 2 (MAP2; Fig. 1*C*). In addition, the absence of OCT4 and NANOG was confirmed at this stage (Fig. 1*C*). Upon injection into immune-compromised SCID mice, the colonies at early passages failed to generate intratesticular teratoma (Fig. S3*C*), further suggesting that the conversion process was direct. Next, we observed that coinfecting CB cells with Sox2 and c-Myc increased the frequency of colonies by 15- to 25-fold (conversion efficiency, 0.06–0.1%; Fig. 1*D*). Thus, although c-Myc is not formally required for the neural conversion process, it does enhance its efficiency dramatically (25). This is in accordance with the known role of c-Myc in controlling the self-renewal and proliferation of neural progenitor cells (26–28). Consistently, we confirmed that Sox2/c-Myc-induced colonies highly expressed TUJ-1, MAP2, DCX, and PAX6 (Fig. 1*E*). In particular, the expression of TUJ-1, NeuroD1, and DCX was predominant and homogeneous in all the clones, whereas a minor variability was observed in the expression level of MAP2, NF, and PAX6 among different clones (Fig. S4*A*). A more extensive characterization of these colonies revealed the lack of expression of early neural markers Nkx2.2, Musashi1, Mash1, and Sox1, whereas low level of expression of Nestin was detected. Moreover, little or no expression of other postmitotic neural markers was seen (NeuN, VGlut1, GABA, and Synapsin1) when colonies were cultured in the presence of bFGF. Finally, no astrocytes or oligodendrocytes were detected under these culture conditions as assessed by GFAP, S100b, OLIG1, PDGFRa, and NG2 immunostaining (Fig. S4 *A* and *B*). Accordingly, when the colonies were disaggregated and replated as single cells onto matrigel-coated plates in neuronal medium, the cell population comprised 44% TUJ-1$^+$ cells and 21% PAX6$^+$ cells (Fig. S4*C*), indicative of an intrinsic bias of these cells toward neuronal differentiation. Thus, these data show that Sox2 and c-Myc in combination with permissive culturing conditions drive the conversion of CB CD133$^+$ cells into a heterogeneous population of CB-iNCs at different levels of neuronal specification and maturation.

CB-iNCs Show Proliferative Activity and Can Be Propagated in Defined Condition Culture. Interestingly, we observed that CB-iNCs could be expanded and maintained in culture on top of HFF-1 and in the presence of bFGF for many passages, without losing their neuronal phenotype (tested for as many as 25 passages). Accordingly, BrdU incorporation along with Ki67 staining showed that the colonies comprised proliferative DCX$^+$/TUJ-1$^+$ cells (Fig. S5*A*).

In an attempt to enrich the proliferating neural progenitors present within CB-iNCs, we performed single-cell clonal assay and observed the presence of a small number of clonogenic cells (~8%), responsible for colony formation. In particular, when CB-iNCs were seeded as single cells on HFF-1 and in the presence of bFGF, we observed the generation of adherent neural epithelium-like colonies (Fig. S5*B*). These cells could be continuously passaged (up to passage 6, at time of manuscript submission) and showed a fast cycling profile when transferred on matrigel and cultured in the presence of bFGF (Fig. S5*C*). Immunostaining revealed that these cells homogeneously expressed early neural progenitor markers NESTIN and SOX2, and the proliferating marker Ki67 (Fig. S5*D*). Accordingly, qRT-PCR analysis showed a down-regulation of markers of more committed neural cells (NeuroD1 and MAP2) and confirmed the up-regulation of early neural markers (Mash1 and Nestin) when these cells were compared with CB-iNCs. In addition, we observed a significant up-regulation of endogenous Sox2, whereas the exogenous Sox2 became silenced (Fig. S6*A*). Interestingly, the up-regulation of neural progenitor markers and endogenous Sox2, as well as the silencing of the transgene, became more pronounced, when the clonal adherent CB-iNCs were cultured under a chemically defined condition previously shown to promote self-renewal of primitive neural precursors (29). Together these data suggest that CB-iNCs contain a small population of early NP-like cells that are capable of self-renewal and have undergone epigenetic changes that reactivated master regulators of neural progenitor fate.

We successfully repeated the experiments with 15 independent CB units by using the two conditions (Sox2 alone and Sox2/c-Myc) and generated 40 CB-iNC lines. Cytogenetic analysis showed that the CB-iNCs lines maintained a normal 46,XY or 46,XX karyotype after more than 15 passages (Fig. S6*B*). Eighteen lines were expanded and characterized for expression of neural markers. Furthermore, seven independent CB-iNC lines were further differentiated into mature neuronal cells and explored for neural activity in vitro and in vivo.

CB-iNCs Differentiate and Show Mature Neuronal Properties. To test their ability to derive functional neurons, CB-iNCs were disaggregated and replated as single cells onto polyornithine/laminin-coated plates or in coculture with human astrocytes, in the presence of neural differentiation medium, for 4 to 6 wk as previously described (30). Although we found that CB-iNCs under both culture conditions acquired morphology typical of

CELL BIOLOGY

Downloaded at Palestinian Territory, occupied on December 18, 2021
www.manaraa.com

mature neurons, the use of astrocyte feeders seemed more effective in directing the maturation and expression of proteins involved in synaptic transmission. After 1 mo, the cells showed MAP2-positive dendrites with distinct vesicular glutamate transporter-1 (VGLUT1) puncta (Fig. 2*A*) or, alternatively, TUJ-1$^+$ processes expressed inhibitory GABAergic markers (Fig. 2*B*). In addition, the appearance of Synapsin puncta on TUJ-1–positive cells highlighted the presence of mature synaptic buttons on CB-derived neurons (Fig. 2*C*). Thus, the presence of Synapsin-positive terminals suggested that these neurons in culture were mature, and the expression of VGLUT1 and GABA markers indicated the presence of inhibitory and excitatory neurons. We successfully repeated the in vitro differentiation of CB-iNCs into neurons by using clones at early and late passages (5–15), without observing any significant difference.

Next, to further characterize the CB-iNCs at the molecular level, we performed a global gene expression analysis on CB-iNCs colonies, CB-derived neurons, and the starting population of selected CB CD133$^+$ cells. Because finding an appropriated positive control is usually difficult when working with human samples, we used human ES (hES)-derived (HUES6)-NPCs and HUES6-neurons as points of reference (30). Consistent with their neuronal phenotypes, CB-iNCs and CB-neurons clustered with HUES6-NPCs and HUES6-neurons rather than with their CD133$^+$ cells of origin (Fig. 2 *D* and *E*). A set of neuronal-specific genes comprising Map2, Pax6, NF, NeuroD1, Ncam1, VGlut1, Map1B, and Synapsin1 was found significantly up-regulated (twofold change; $P < 0.05$) in CB-iNCs and CB-derived neurons in comparison with the starting population CB CD133$^+$ cells (Fig. 2*E*). As controls, the down-regulation of hematopoietic-specific genes (CD34, CD38, CD31, CD45, Flt3, and Gata2) in CB-iNCs indicated that they had undergone an erasure of their hematopoietic transcriptional profile.

To gain further insights into the underlying mechanism of the role of Sox2 during the conversion process, we investigated whether genes up-regulated in CB-iNCs, which are known to have potential SOX2 binding sites (19, 31), were also bound by SOX2 in CB-iNCs. By using ChIP, we found evidence that SOX2 binds the NeuroD1, Dcx, Nav2, Mash1, and Chd7 genes (Fig. 2*F*).

We performed Southern blot analysis of genomic DNA and confirmed the independent origin of our CB-iNCs and showed a maximum of two integrations per retrovirus and genome in all CB-iNCs clones analyzed (Fig. S7*A*). qRT-PCR analysis showed that exogenous Sox2 and c-Myc were expressed in CB-iNCs colonies, although, following neuronal differentiation, we observed a significant down-regulation of the retroviral transgenes (Fig. S7*B*).

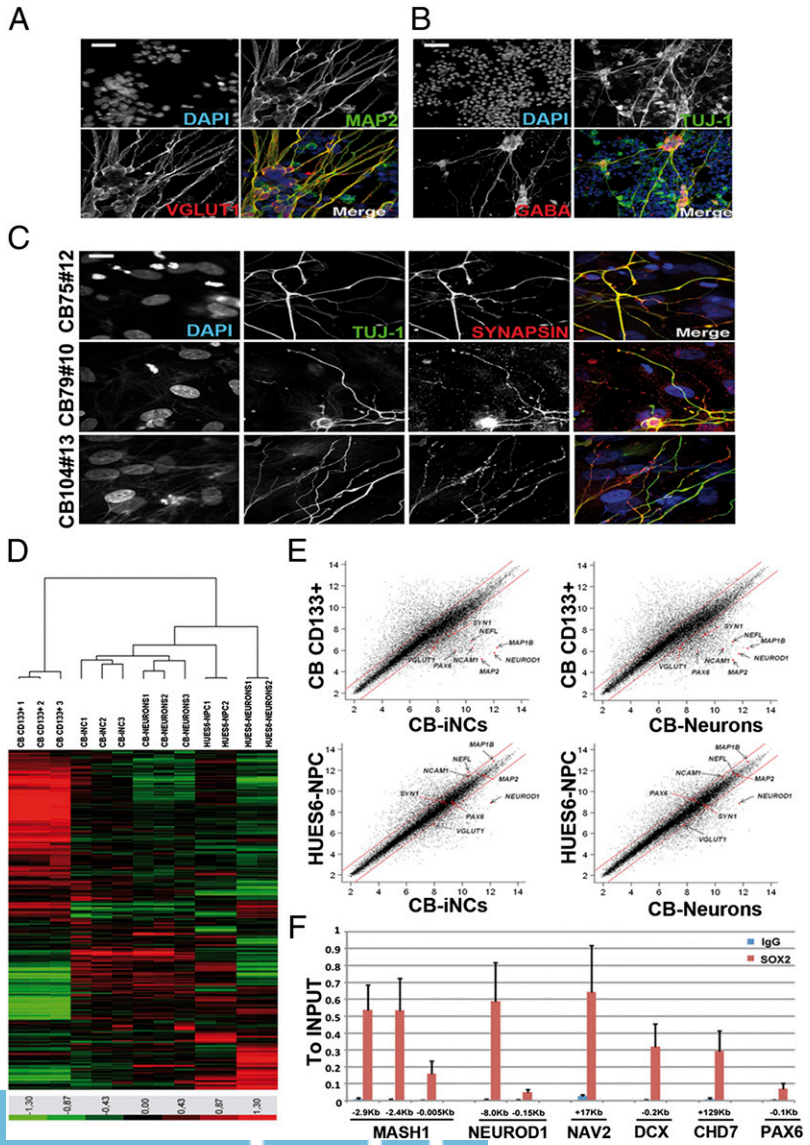

Fig. 2. Characterization and gene-expression profile of CB-derived neurons. (*A*) CB-iNCs after 6 wk of differentiation on top of human astrocytes acquired a more mature phenotype highlighted by the expression of the excitatory markers VGLUT1 and the dendritic marker MAP2. (Scale bar, 30 μm.) (*B*) CB-derived neurons were positive for inhibitory markers such as GABA. (Scale bar, 80 μm.) (*C*) Synaptic buttons on CB-derived neurons were highlighted by the expression of synapsin puncta on TUJ-1–positive cells. (Scale bar, 10 μm.) (*D*) Heat map of genes differentially expressed in microarray analysis performed on CB CD133$^+$ cells, CB-iNCs, and CB-derived neurons. Human ES-derived (HUES6) NPCs and HUES6-derived neurons were used as points of reference for neuronal phenotype. (*E*) Average global gene expression patterns were compared between CB CD133$^+$ (n = 3 replicates) CB-iNCs (n = 3 replicates), CB-derived neurons (n = 3 replicates), and HUES6-NPCs (n = 2 replicates). Some neural-specific genes are highlighted in the plots (*Map1*, *Map2*, *VGlut1*, *Pax6*, *NF*, *NeuroD1*, *Ncam*, and *Synapsin1*). We found up-regulation of Fez1, Tead2, and NNAT, typical markers for dorsal neurons. (*F*) ChIP assay shows SOX2 binding to the regulatory regions of the indicated genes. Levels were determined by quantitative PCR and are expressed as fold change vs. the input. The positions of the amplicons are indicated in kilobases from the transcription start site (TSS). The mean and SD of three independent experiments is shown.

Downloaded at Palestinian Territory, occupied on December 18, 2021
www.manaraa.com

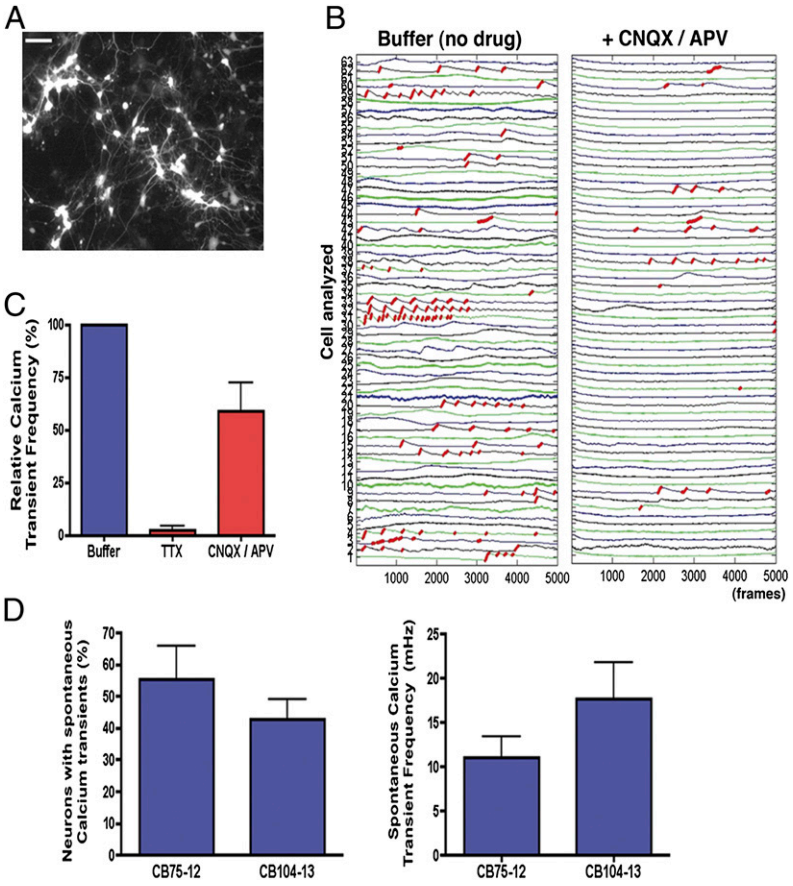

Fig. 3. Activity-dependent calcium transients in CB-derived neurons. (*A*) Representative example of Syn::DsRed cultures of CB-derived mature neurons used for calcium signal traces. (Scale bar, 50 μm.) (*B*) Red traces correspond to the calcium rise phase detected by the algorithm used (*SI Materials and Methods*). Example of fluorescence intensity changes reflecting intracellular calcium fluctuations in CB-derived neurons before and after glutamate receptor antagonist (CNQX/APV) treatment. Each number on the left corresponds to the tracing of a different neuron on the plate. (*C*) Effects of TTX (1 μM) and CNQX/APV (10 μM/20 μM) on intracellular calcium transient frequency of individual neurons analyzed simultaneously by calcium imaging. (*D*) Analysis of spontaneous intracellular calcium transients in CB-derived neurons after 4 wk of differentiation. CB-derived neurons differentiated from two distinct CB-iNCs showed similar prevalence of calcium signaling as well as similar transient frequency within the neuronal population. Data shown as mean ± SEM.

To assess whether the CB-iNCs can be stably maintained without continued transgene expression, we used a doxycycline-inducible strategy to generate CB-iNCs (Fig. S7 *C–E*). The colonies were then cultured in the presence of bFGF but with decreasing doxycycline concentrations. These data showed that CB-iNCs achieved a stable neuronal state independent of viral transgene expression and could be expanded as many as 15 passages after doxycycline withdrawal without loss of the neuronal phenotype (Figs. S7*E* and S8 *A* and *B*). We confirmed the presence of mitotic Ki67$^+$/TUJ-1$^+$/DCX$^+$ cells in the complete absence of transgene activity (Fig. S8*C*).

CB-Derived Neurons Show Synaptic Activity in Vitro. Electrical cell activity leads to increases in intracellular calcium levels and activation of signaling pathways that are important for the regulation of processes in neurons (32). First, to test if CB-derived neuronal networks were functionally capable of generating calcium transients, we preloaded the cells with the calcium indicator fluo-4AM and highlighted neurons using the Synapsin::DsRed reporter (Fig. 3*A*). Cultures with similar density and number of DsRed-positive neurons were used. Spontaneous calcium transients were detected in neuronal networks that were generated from two independent CB-iNC lines (Fig. 3 *B–D*). Calcium transients detected in CB-derived neurons were blocked after the addition of glutamate receptor antagonists [6-cyano-7-nitroquinoxaline-2,3-dione (CNQX; AMPA receptor antagonist) and (2R)-amino-5-phosphonovaleric acid (APV; NMDA receptor antagonist); Fig. 3*B*] and after the addition of TTX (Fig. 3*C*), indicating that the recorded activities are specifically dependent on local synaptic connections.

Whole-cell recording was performed on cells that had differentiated 6 to 8 wk in coculture with human primary astrocytes. CB-derived neurons were visualized by infection with the Synapsin::DsRED or Synapsin::GFP lentiviral vector (Fig. 4*A*). CB-derived neurons from distinct CB-iNC clones expressed functional voltage-dependent sodium and potassium channels and were able to fire action potentials after current injection (Fig. 4 *B–D*).

CB-Derived Neurons Engraft and Integrate into Mouse Hippocampus. We next tested whether CB-derived neurons were able to integrate into existing neural networks in vivo. To this end, EGFP-expressing CB-iNCs and CB-iNCs differentiated in coculture with human astrocytes for 4 wk were injected into the hippocampus of 14-d-old NOD-SCID mice. We assayed for the presence of EGFP$^+$ cells 2 wk, 1 mo, and 3 mo after transplantation. As shown in Fig. S9, 2-wk transplanted cells expressed neuronal markers TUJ-1 and NEUN and integrated within the host tissue. The integrated CB-iNCs extended processes to endogenous granule neurons of the dentate gyrus as well as along the mossy fiber path to pyramidal neurons in the CA2/CA3 regions, and were able to integrate along the corpus callosum, sending extensive TUJ-1$^+$ processes to the contralateral hemisphere.

As a negative control, CB CD133$^+$ cells infected only with a constitutive EGFP lentivirus and transplanted into the hippocampus of 14-d-old mice were not able to differentiate into neurons in vivo. They exhibited a round morphology with no processes and were negative for TUJ-1 (Fig. 4*E*).

We found that, at 1 mo after transplantation, 90% of the CB-derived neurons grafted were positive for TUJ-1 and 48% were positive for the mature neuronal marker NEUN (Fig. 4 *F–H*). In contrast, very few EGFP$^+$ CB CD133$^+$ cells survived in the transplanted animals 4 wk after injection, further confirming that CB CD133$^+$ cells do not have intrinsic neurogenic potential in vivo. Instead, CB-derived neurons survived at least 3 mo in the transplantation site and developed long dendritic processes bearing PSD95 puncta (Fig. S9*D*), suggestive of possible interactions with the host cells. We performed electrophysiological recordings on mouse brain sections 3 mo after transplantation

Downloaded at Palestinian Territory, occupied on December 18, 2021
www.manaraa.com

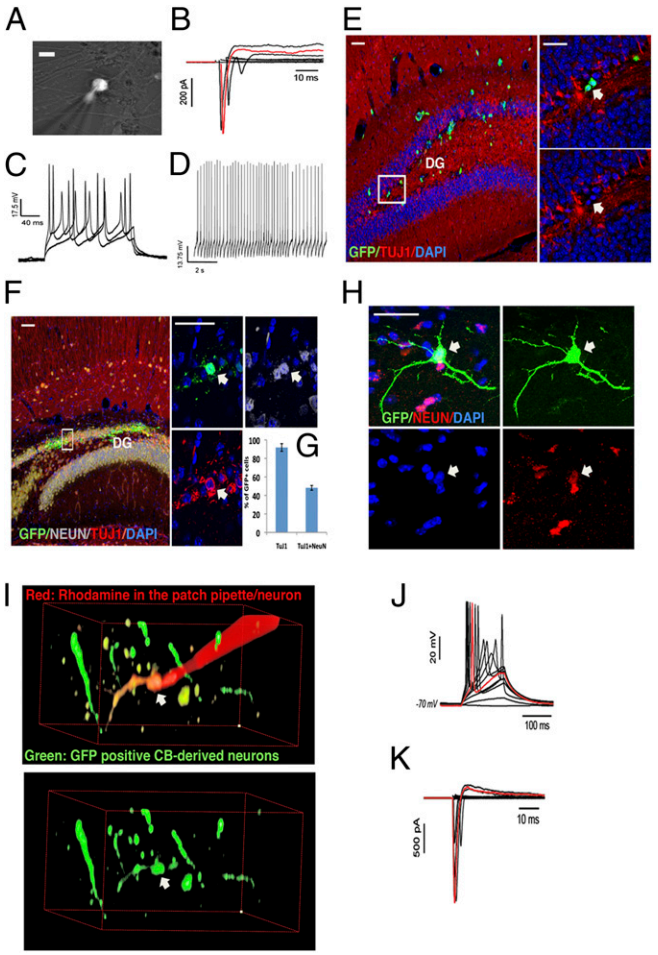

Fig. 4. Electrophysiology and in vivo grafting of CB-derived neurons. (*A*) Representative fluorescence micrograph of CB-derived neurons in culture expressing Synapsin::DsRed. (Scale bar, 10 μm.) (*B* and *C*) Whole-cell recordings obtained in vitro. (*B*) Transient Na^+ currents and sustained K^+ currents in response to voltage step (cell voltage-clamped at −70 mV while transient steps at 5-mV increments were applied). The trace highlighted in red was obtained in response to a step of +45 mV from resting −70 mV. (*C*) Action potentials evoked by somatic current injections (cell current-clamped at approximately −70 mV, currents from 50 to 150 pA at 50-pA steps). (*D*) Spontaneous action potentials when the cell was current-clamped at −60 mV. (*E*) $CD133^+$ cells grafted in the hippocampus, as controls, did not integrate into the host tissue and did not express the neuronal markers TUJ-1 (arrow). (*F*) Representative image of CB-derived neurons 4 wk after transplantation show increase in colocalization with the mature neuronal marker NEUN (arrow). (Scale bars, 50 μm.) (*G*) Quantification of percentage of CB-derived neurons positive for TUJ-1 and NEUN 4 wk after transplantation. (*H*) Detail of a GFP^+ CB-derived neuron 3 mo after transplantation shows extensive arborization and colocalization with the mature neuronal marker NEUN. (Scale bar, 50 μm.) (*I–K*) Whole-cell recordings obtained from a GFP^+ CB-derived neuron 3 mo after its transplantation in a young mouse hippocampus from cell represented in *I* demonstrate that CB-derived neural progenitors can develop into functional neurons and survive in the mouse brain. (*J*) Action potentials evoked by somatic current injections [cell current-clamped at approximately −70 mV (−2 pA) while increments of 2 pA were applied]. (*K*) Transient Na^+ currents and sustained K^+ currents in response to voltage step (cell voltage-clamped at −70 mV while transient steps at 5-mV increments were applied). The traces highlighted in red were obtained in response to steps of +20 pA (*J*) or +45 mV (*K*).

and found that GFP-positive CB-derived neurons were able to fire action potentials (Fig. 4 *I–K*).

Although spontaneous or evoked postsynaptic current could not be recorded, the electrophysiological recordings, together with the calcium imaging data, strongly indicate that CB-derived neurons exhibited functional neuronal properties in vitro and in vivo.

Discussion

This study shows the direct conversion of a pure population of human blood cells ($CD45^+/CD133^+$) into cells of the neuronal lineage by forced expression of only one transcription factor. Here we successfully demonstrate that cells from the mesodermal lineage can be switched to an ectodermal fate.

A major concern associated with the direct conversion of somatic cells is that rare contaminating NP or NC cells could be present in the starting population and selectively expanded when culture under neural culture conditions. To exclude definitively this possibility, we confirmed that our starting population did not contain any cells positive for NP (Nestin, Sox1, Nkx2.2, GFAP) and NC (Sox10 and p75) markers.

From a more mechanistic point of view, it has been described that the use of iPSC transcription factors in lineage conversion experiments might first induce the generation of an unstable pluripotent state (10, 24). CB-iNCs were derived by forced expression of Sox2 in combination with human ES/iPSC condition cultures; however, the omission of Oct4 during the conversion process ruled out the possibility that intermediate pluripotent stages were generated. Our data are in agreement with a recent study by Han et al. that shows the direct conversion of mouse fibroblasts into NSCs by forced expression of five transcription factors, including Sox2, c-Myc, and Klf4, but not Oct4 (13). Furthermore, we find that CB-iNCs exhibit a neuron-restricted phenotype already at the earliest passages, which is consistent with the strong activation of proneuronal markers such as PAX6, NeuroD1, DCX, TUJ-1, MAP2, and NF. Instead, glial marker expression was virtually absent in these clones. These data are indicative that CB-iNCs contain a heterogeneous population of neuronal-like cells at different stages of neuronal specification, which show proliferative activity when cultured in permissive condition culture. Accordingly, we show that CB-iNCs contain a small population of neural progenitor-like cells that are capable of self-renewal and that may resemble the population of ($Nestin^{+/-}/GFAP^-/Sox2^+/Dcx^+$) transient amplifying neuron-restricted progeny recently described in adult hippocampal neurogenesis (33). Furthermore, we show that CB-iNCs can mature to the point of exhibiting functional neuronal properties as judged by the measurement of action potential. Although CB-iNCs exhibit a series of neural properties, including the ability to engraft and differentiate into mature neurons after transplantation, these cells could not generate spontaneous postsynaptic activity. To this end, it is conceivable that further optimization of the culturing conditions will lead to the generation of fully mature neurons. However, our data are perfectly in line with previous works describing the derivation of human iNCs (30, 34, 35), and support the idea that in general human cells are less plastic and require longer maturation compared with mouse cells (36, 37).

One strength of our protocol in comparison with others that have achieved the direct conversion of human fibroblasts into neurons is the advantage of generating a neural progenitor population that can be further expanded and maturated in vitro. The remarkable capability of a single factor to directly convert CB cells into neuronal cells provides further evidence of the plasticity of stem cell populations, which are much more amenable to cell state transitions than somatic cells. This possibility is further corroborated by the lack of neural induction from CD133-negative fraction of CB by using the same approach. These facts highlight the importance of the starting population.

It would be interesting to perform a side-by-side comparison of the reprogramming into iNCs of CB cells vs. human fibroblasts to understand the role of key transcription factors and to determinate the impact of donor cell type. Thus, CB-iNCs provide a complementary paradigm for the conduction of mechanistic studies on transdifferentiation and drug screening, which nor-

Downloaded at Palestinian Territory, occupied on December 18, 2021
www.manaraa.com

mally require a reproducible induction strategy along with relatively high numbers of cells.

Materials and Methods

CD133$^+$ Cell Purification. CB samples were obtained from the Banc de Sang i Teixits, Hospital Duran i Reynals, Barcelona, Spain. Mononuclear cells were isolated by using density gradient centrifugation. CD133$^+$ cells were selected by using an immunomagnetic separation system (Miltenyi Biotec). Purification efficiency was verified by flow cytometric analysis staining with CD133 (phycoerythrin; Miltenyi Biotec) and CD45 (allophycocyanin; Becton Dickinson) antibodies. The CB CD133$^+$ cells were infected and cultured as previously described (14, 23) (*SI Materials and Methods*).

CB-iNC Generation and Culture. CD133$^+$ after infection were cultured on top of HFF-1 in the presence of hES medium and 20 ng/mL bFGF (Peprotech). Three weeks after infection, CB-iNC colonies started to appear. For expansion, CB-iNC colonies were maintained on top of HFF-1 in the presence of hES medium and 20 ng/mL bFGF (Peprotech) and picked mechanically every 7 d.

CB-iNC Differentiation into Mature Neurons. CB-iNCs were dissociated by using trypsin, and 10,000 single cells were plated on human cerebellar astrocytes (ScienCell) on polyornithine/laminin-coated plates in the presence of DMEM/F12 plus N2 and B27 supplements, retinoic acid (1 μM), brain-derived neurotrophic factor, glial cell line-derived neurotrophic factor (both at 20 ng/mL), Lam (1 μg/mL), 200 nM ascorbic acid (Sigma), 1 mM dibutyryl-cAMP Lam (1 μg/mL), and 0.5% FBS for 6 wk. For immunofluorescence assay, cells were fixed in 4% (wt/vol) paraformaldehyde in PBS solution for 20 min. The antibodies used to stain CB-derived neurons were TUJ-1 (1:500; Covance), MAP2 (1:100; Sigma), VGLUT1 (1:200; Synaptic Systems), GABA (1:100; Sigma), synapsin (1:400; Calbiochem), and EGFP (1:200; Invitrogene).

Functional in Vitro and in Vivo Studies. Similar methods were used for in vitro culture experiments and ex vivo slice experiments. Individual coverslips or slices for were transferred into a heated recording chamber and continuously perfused (1 mL/min) with bubbled artificial cerebrospinal fluid maintained at 25 °C. For targeted whole-cell recordings, we used a 40× water-immersion objective, differential interference contrast filters (Olympus), a digital camera (Rolera XR; Qimaging), a halogen bulb (Olympus), a Digidata 1440A/Multiclamp 700B amplifier and Clampex 10.3 software for analysis (Molecular Devices). For measurement of voltage-gated Na^+ currents, cells were clamped at −70 mV and stimulated by step depolarizations of 300 ms (command voltage from −55 to 0 mV in 5-mV steps). Cells were current clamped at -70 mV to measure the spiking activities in response to somatic current injections (duration of 300 ms, currents starting from 50 pA in 50-pA increments). For ex vivo experiments, patching of deep GFP$^+$ cells was also assisted with a two-photon laser scanning system (FV1000MPE; Olympus). The resistance of the patch electrodes was between 3 and 5 MΩ. Patch electrodes were filled with internal solutions containing 130 mM K-gluconate, 6 mM KCl, 4 mM NaCl, 10 mM Na-Hepes, 10 mM D-glucose, nucleotides (0.3 mM GTP, 2 mM Mg-ATP, and 0.2 mM cAMP), 0.2 mM K-EGTA, 0.15% biocytin, and 0.06% rhodamine. The pH and osmolarity of the internal solution were close to physiological conditions (pH 7.3, 290–300 mOsm). Data were all corrected for liquid junction potentials (10 mV). Electrode capacitances were compensated online in cell-attached mode (~7 pF). Recordings were low-pass filtered at 2 kHz, digitized, and sampled at intervals of 50 μs (20 kHz). To control the quality and the stability of the recordings throughout the experiments, access resistance, capacitance, and membrane resistance were continuously monitored online.

ACKNOWLEDGMENTS. The authors thank Rosario Sànchez-Pernaute, Nuria Montserrat, Federico Gonzalez Grassi, Emmanuel Nivet, Ava Carter, Ignacio Sancho-Martinez, and Leopoldo Laricchia-Robbio for conceptual advice as well as critical comments; Sachin Kumar, Na Young Kim, and Ilir Dubova for help with molecular characterization of cord blood-derived neurons; José Miguel Andrés Vaquero for assistance with flow cytometry; and Lola Mulero Pérez, Cristina Morera, and Mercé Gaudes Martí for bioimaging assistance. This study was supported by California Institute for Regenerative Medicine Grants RL1-00649-1 and RC1-00115-1 (to F.H.G.), the Lookout Fund (F.H.G.), the Mathers Foundation (F.H.G.), the Helmsley Foundation (F.H.G.), the JPB Medical Foundation (F.H.G.), Ministerio de Economía y Competitividad, Fundacion Cellex, Sanofi, the G. Harold and Leila Y. Mathers Charitable Foundation (J.C.I.B.), and the Leona M. and Harry B. Helmsley Charitable Trust (J.C.I.B.). C.B. is a Seventh Framework Programme Marie Curie International Outgoing Fellow.

1. Takahashi K, Yamanaka S (2006) Induction of pluripotent stem cells from mouse embryonic and adult fibroblast cultures by defined factors. *Cell* 126:663–676.
2. Vierbuchen T, et al. (2010) Direct conversion of fibroblasts to functional neurons by defined factors. *Nature* 463:1035–1041.
3. Pang ZP, et al. (2011) Induction of human neuronal cells by defined transcription factors. *Nature* 476:220–223.
4. Caiazzo M, et al. (2011) Direct generation of functional dopaminergic neurons from mouse and human fibroblasts. *Nature* 476:224–227.
5. Ambasudhan R, et al. (2011) Direct reprogramming of adult human fibroblasts to functional neurons under defined conditions. *Cell Stem Cell* 9:113–118.
6. Son EY, et al. (2011) Conversion of mouse and human fibroblasts into functional spinal motor neurons. *Cell Stem Cell* 9:205–218.
7. Marro S, et al. (2011) Direct lineage conversion of terminally differentiated hepatocytes to functional neurons. *Cell Stem Cell* 9:374–382.
8. Yoo AS, et al. (2011) MicroRNA-mediated conversion of human fibroblasts to neurons. *Nature* 476:228–231.
9. Pfisterer U, et al. (2011) Direct conversion of human fibroblasts to dopaminergic neurons. *Proc Natl Acad Sci USA* 108:10343–10348.
10. Kim J, et al. (2011) Direct reprogramming of mouse fibroblasts to neural progenitors. *Proc Natl Acad Sci USA* 108:7838–7843.
11. Lujan E, Chanda S, Ahlenius H, Südhof TC, Wernig M (2012) Direct conversion of mouse fibroblasts to self-renewing, tripotent neural precursor cells. *Proc Natl Acad Sci USA* 109:2527–2532.
12. Thier M, et al. (2012) Direct conversion of fibroblasts into stably expandable neural stem cells. *Cell Stem Cell* 10:473–479.
13. Han DW, et al. (2012) Direct reprogramming of fibroblasts into neural stem cells by defined factors. *Cell Stem Cell* 10:465–472.
14. Giorgetti A, et al. (2009) Generation of induced pluripotent stem cells from human cord blood using OCT4 and SOX2. *Cell Stem Cell* 5:353–357.
15. Kim JB, et al. (2009) Direct reprogramming of human neural stem cells by OCT4. *Nature* 461:649–3.
16. Rocha V, et al.; Acute Leukemia Working Party of European Blood and Marrow Transplant Group; Eurocord-Netcord Registry (2004) Transplants of umbilical-cord blood or bone marrow from unrelated donors in adults with acute leukemia. *N Engl J Med* 351:2276–2285.
17. Gluckman E, Rocha V (2009) Cord blood transplantation: State of the art. *Haematologica* 94:451–454.
18. Graham V, Khudyakov J, Ellis P, Pevny L (2003) SOX2 functions to maintain neural progenitor identity. *Neuron* 39:749–765.
19. Cimadamore F, et al. (2011) Human ESC-derived neural crest model reveals a key role for SOX2 in sensory neurogenesis. *Cell Stem Cell* 8:538–551.
20. Pevny LH, Nicolis SK (2010) Sox2 roles in neural stem cells. *Int J Biochem Cell Biol* 42:421–424.
21. Zangiacomi V, et al. (2008) Cord blood-derived neurons are originated from CD133+/CD34 stem/progenitor cells in a cell-to-cell contact dependent manner. *Stem Cells Dev* 17:1005–1016.
22. Domanska-Janik K, Buzanska L, Lukomska B (2008) A novel, neural potential of non-hematopoietic human umbilical cord blood stem cells. *Int J Dev Biol* 52:237–248.
23. Giorgetti A, et al. (2010) Generation of induced pluripotent stem cells from human cord blood cells with only two factors: Oct4 and Sox2. *Nat Protoc* 5:811–820.
24. Szabo E, et al. (2010) Direct conversion of human fibroblasts to multilineage blood progenitors. *Nature* 468:521–526.
25. Nakagawa M, et al. (2008) Generation of induced pluripotent stem cells without Myc from mouse and human fibroblasts. *Nat Biotechnol* 26:101–106.
26. Kerosuo L, et al. (2008) Myc increases self-renewal in neural progenitor cells through Miz-1. *J Cell Sci* 121:3941–3950.
27. Kerosuo L, et al. (2010) CIP2A increases self-renewal and is linked to Myc in neural progenitor cells. *Differentiation* 80:68–77.
28. Wey A, Martinez Cerdeno V, Pleasure D, Knoepfler PS (2010) c- and N-myc regulate neural precursor cell fate, cell cycle, and metabolism to direct cerebellar development. *Cerebellum* 9:537–547.
29. Li W, et al. (2011) Rapid induction and long-term self-renewal of primitive neural precursors from human embryonic stem cells by small molecule inhibitors. *Proc Natl Acad Sci USA* 108:8299–8304.
30. Marchetto MC, et al. (2010) A model for neural development and treatment of Rett syndrome using human induced pluripotent stem cells. *Cell* 143:527–539.
31. Engelen E, et al. (2011) Sox2 cooperates with Chd7 to regulate genes that are mutated in human syndromes. *Nat Genet* 43:607–611.
32. Spitzer NC, Root CM, Borodinsky LN (2004) Orchestrating neuronal differentiation: patterns of Ca2+ spikes specify transmitter choice. *Trends Neurosci* 27:415–421.
33. Encinas JM, et al. (2011) Division-coupled astrocytic differentiation and age-related depletion of neural stem cells in the adult hippocampus. *Cell Stem Cell* 8:566–579.
34. Qiang L, et al. (2011) Directed conversion of Alzheimer's disease patient skin fibroblasts into functional neurons. *Cell* 146:359–371.
35. Johnson MA, Weick JP, Pearce RA, Zhang SC (2007) Functional neural development from human embryonic stem cells: accelerated synaptic activity via astrocyte coculture. *J Neurosci* 27:3069–3077.
36. Yang N, Ng YH, Pang ZP, Südhof TC, Wernig M (2011) Induced neuronal cells: how to make and define a neuron. *Cell Stem Cell* 9:517–525.
37. Vierbuchen T, Wernig M (2011) Direct lineage conversions: Unnatural but useful? *Nat Biotechnol* 29:892–907.

Downloaded at Palestinian Territory, occupied on December 18, 2021

www.manaraa.com